Performance Analysis of a Conical Hydrodynamic Journal Bearing

Ajay Kumar Gangrade, Vikas M. Phalle & S. S. Mantha

Iranian Journal of Science and Technology, Transactions of Mechanical Engineering

ISSN 2228-6187

Iran J Sci Technol Trans Mech Eng
DOI 10.1007/s40997-018-0217-2

Springer

Iran J Sci Technol Trans Mech Eng
https://doi.org/10.1007/s40997-018-0217-2

RESEARCH PAPER

Performance Analysis of a Conical Hydrodynamic Journal Bearing

Ajay Kumar Gangrade[1] · Vikas M. Phalle[1] · S. S. Mantha[1]

Received: 3 October 2017 / Accepted: 21 June 2018

Abstract
Many turbo-machines such as turbines and compressors generate axial and radial load during their operation. Conical hydrodynamic journal bearing is proposed to sustain radial load and adjust the effect of axial load on rotating elements. The present study has proposed the performance analysis for conical hydrodynamic journal bearing of semi-cone angles (γ = 5°, 10°, 20°, 30°) for a wide range of radial load ($\bar{W}_r = 0.1 - 0.9$) on rotating journal. Finite element method has been used to solve the modified Reynolds equation for investigating the flow of lubricant in the clearance space between journal and bearing. Performance characteristics such as load-carrying capacity, fluid film thickness, stiffness coefficients, damping coefficients and threshold speed for various configurations of conical hydrodynamic journal bearing have been presented and discussed. Results show that threshold speed ($\bar{\omega}_{th}$) of conical journal bearing is considerably reduced as the semi-cone angle increases to γ = 30° as compared to the base bearing of semi-cone angle γ = 5°.

Keywords Conical journal bearing · Hydrodynamic lubrication · Aspect ratio · FEA

List of symbols

C_{ij}	Damping coefficient (i, j = 1,2) (Ns/m)
c_r	Radial clearance (μm)
c_r/R_j	Clearance ratio
D	Mean bearing diameter (mm)
d	Mean journal diameter (mm)
e	Journal eccentricity (mm) ($e^2 = x^2 + z^2$)
$e_o; \varphi_o$	Journal eccentricity and attitude angle at initial equilibrium position
F	Fluid film reaction $\frac{\partial h}{\partial t} \neq 0$ (N)
F_o	Fluid film reaction $\frac{\partial h}{\partial t} = 0$ (N)
F_x, F_z	Fluid film reaction component in X and Z directions, $\frac{\partial h}{\partial t} \neq 0$ (N)
F_a, F_r	Fluid film reaction component in axial and radial directions, $\frac{\partial h}{\partial t} \neq 0$ (N)
h	Fluid film thickness (mm)
h_{min}	Minimum fluid film thickness (mm)
L	Bearing length (mm)
o_1, o_2	Bearing and journal center
p	Fluid film pressure (MPa)
p_{max}	Maximum fluid film pressure (MPa)
p_s	Supply pressure (MPa)
R_b	Mean bearing radius (mm)
R_j	Mean journal radius (mm)
R_1, R_2	Minimum and maximum radius of conical journal (mm)
S_{ij}	Fluid film stiffness coefficients (i, j = 1, 2) (N/m)
t	Time (s)
t_s	Supply temperature (°C)
W	External load (N)
W_a	Axial load (N)
W_r	Radial load (N)
X, Y, Z	Cartesian coordinates (mm)
x, z	Horizontal, vertical journal eccentricity (mm)
$X_j, Z_j; \dot{X}_j, \dot{Z}_j$	Journal center displacement and velocity components
X_J, Z_J	Coordinates of steady-state equilibrium journal center from geometric center of bearing (mm)

✉ Ajay Kumar Gangrade
akgangrade@somaiya.edu

Vikas M. Phalle
vmphalle@gmail.com

S. S. Mantha
ssmantha@vjti.org.in

[1] Machine Dynamics and Vibration Laboratory, Department of Mechanical Engineering, Veermata Jijabai Technological Institute (VJTI), Mumbai 400019, India

Published online: 29 June 2018

Greek symbols

α	Circumferential coordinate (ϕ) (rad)
β	Axial coordinate ($r\sin\gamma/R_j$)
γ	Semi-cone angles
ε	Journal eccentricity ratio (e/c_r)
r, θ, ϕ	Spherical coordinates (mm, rad) ($\theta = \gamma$)
φ	Attitude angle (rad)
λ	Aspect ratio (L/D)
μ	Lubricating fluid absolute or dynamic viscosity (Ns/m^2)
ρ	Mass density of lubricating fluid (kg/m^3)
μ_r	Dynamic viscosity at reference inlet temperature and atmospheric pressure (Ns/m^2)
v	Journal relative velocity (m/s)
ω	Journal angular velocity (rad/s)
Ω	Speed parameter $\omega\left(\mu R_j^2/c_r^2 p_s\right)$

Non-dimensional parameters

$\bar{C}_{11}, \bar{C}_{22}$	Direct damping coefficients
$\bar{C}_{12}, \bar{C}_{21}$	Cross-coupled damping coefficients
$\bar{C}_{ij}$	Damping coefficient
$\bar{h}$	Fluid film thickness (h/c_r)
$\bar{h}_{min}$	Minimum fluid film thickness (h_{min}/c_r)
$\bar{M}_c$	Critical mass parameter $M_c\left(c_r^5 p_s/\mu^2 R_j^6\right)$
N_j	Shape function
ξ, η	Local coordinates system for shape function N_j
$\bar{p}$	Pressure ratio (p/p_s)
$\bar{p}_j$	Pressure ratio at jth nodal point (p_j/p_s)
$\bar{p}_{max}$	Maximum pressure ratio (p_{max}/p_s)
$\bar{S}_{11}, \bar{S}_{22}$	Direct stiffness coefficients
$\bar{S}_{12}, \bar{S}_{21}$	Cross-coupled stiffness coefficients
$\bar{S}_{ij}$	Stiffness coefficient
$\bar{W}_a$	Axial load $\left(\bar{W}_a = \frac{W_a}{p_s R_j^2}\right)$
$\bar{W}_r$	Radial load ($\bar{W}_r = \frac{W_r}{p_s R_j^2}$)
$\bar{\mu}$	Dynamic viscosity (μ/μ_r)
$\bar{\omega}_{th}$	Threshold speed margin
$[\bar{F}]$	Assembled fluidity matrix
$\{\bar{p}\}$	Nodal pressure vector
$\{\bar{Q}\}$	Nodal flow vector
$\{\bar{R}_H\}$	Column vector due to hydrodynamic terms
$\{\bar{R}_{x_j}\}, \{\bar{R}_{z_j}\}$	Global vectors due to journal center linear velocities
$\bar{t}$	Time $t\left(c_r^2 p_s/\mu R_j^2\right)$
$\Delta\bar{X}_J, \Delta\bar{Z}_J$	Small amount of journal movement from steady-state equilibrium journal center
$\bar{X}_J = X_J/C_r, \bar{Z}_J = Z_J/C_r$	Coordinates of steady-state equilibrium journal center
$\Delta\dot{\bar{X}}_J, \Delta\dot{\bar{Z}}_J$	Velocity components of journal center

1 Introduction

Research activities in the area of fluid film conical journal bearings have been increased due to its low cost, compact size and applications in combined axial and radial load conditions. The conical hydrodynamic journal bearings have been recently used in the precision spindle of a rotating machine to replace the journal and thrust hydrodynamic bearings (Kim et al. 2017; Krzysztof 2008). These bearings also provide better suitability for rotating shaft by adjustment of clearance space between rotor and bearing. Conical journal bearings are also utilized to support rotors in a wide range of rotating machinery, varying from micro-electro-mechanical systems (MEMS) to hydro-turbines of capacity more than 100 MW (Chen 2012).

Many researchers have investigated the performance of conical journal bearing system. Korneev et al. (2010) and Korneev and Yaroslavtsev (2010) proposed the formulae for load-carrying capacity and variation in dynamic coefficients of the lubricant layer for the dynamic characteristics of conical multipad hydrodynamic liquid friction bearings. From their study, it has been observed that dynamic characteristics of the conical multipad hydrodynamic bearing depend on relative radial eccentricity, speed and taper angle. Gamal and Al-Hanaya (2014) studied the fluid flow in the immobile conic surfaces using averaged clearance method based on the thin film model to solve the pressure distribution equation. They have presented numerical results in the form of non-dimensional charts for radial and axial load-carrying capacity of bearing. In another study, Korneev (2014) used a special program to plot the rotor trajectories in order to determine the stability of the system for conical hydrodynamic bearings using geometric parameters and various operating conditions.

Murthy (1981) carried out the experimental work to analyze the performance of conical hydrodynamic crown bearing and found that different lobe configuration of bearings improves the stability of the bearing. Ettles and Svoboda (1975) studied the application of double-conical journal bearings in high-speed centrifugal pump and stated

the limitations of double-inclined journal bearing. They have also discussed the effect of aspect ratio on stability of circular bearing. Further, Sumikura et al. (2005, 2006) conducted the experiments on conical hydrodynamic journal bearings for axial flow blood pump, which can be used in medical science applications and found that conical bearing provides an excellent load-carrying capacity with reducing fluid film thickness. Heshmat et al. (2006) reviewed the performance of conical hydrodynamic journal bearings and reported that taper-land configuration of bearing geometry had a significant influence on load-carrying capacity of hydrodynamic journal bearing. Very recently, Sharma et al. (2011a, b) analyzed the static and dynamic performance analysis of conical hydrostatic/hybrid journal bearing using modified Reynolds equation and Newton–Raphson method. They have also developed a code to compute the performance of bearing by using finite element method. Kirk and Guntur (1976) demonstrated the minimum influence of cross-coupling damping coefficients on the performance of hydrodynamic journal bearing as compared to cross-coupled stiffness coefficients. Mehrjardi et al. (2016) used the finite element method for stability performance characteristics of circular and non-circular journal bearings for different values of eccentricity ratio. Result from their studies shows that by increasing the eccentricity ratio for a constant external load, the whirl frequency ratio increases, where as critical mass parameter decreases.

Benasciutti et al. (2012) used numerical approach based on perturbation method to compute stiffness and damping matrices for static and dynamic analysis of hydrodynamic radial journal bearings. They also showed the influence of deformation in bearing components on oil pressure distribution and compared the results with rigid components in bearing. Further, Hong et al. (2009) discussed the effect of rotational speed and eccentricity ratio on dynamic coefficients of the hybrid conical journal bearing using theoretical and experimental methods. Kim et al. (2012) used the finite element formulation to calculate the load, stiffness, and damping coefficients for fluid dynamic bearings (FDBs) of various configurations such as journal, thrust, conical and spherical. Papadopoulos et al. (2008) solved the Reynolds equation using finite element method and presented the results in terms of dynamic coefficients of rotor bearing. The result demonstrated in the study of Luis (2010) shows that the hydrodynamic journal bearing stability performance is improved with the increase in eccentricity ratio and found it stable at eccentricity ratio of 0.75 and above for all aspect ratios of bearings. The previous studies of other researchers (Ferron et al. 1983; Jagadeesha et al. 2012; Bouyer and Fillon 2011; Cong and Khonsari 2013) confirmed that the performance of fluid film bearings is dependent on bearing geometrical configuration, operating conditions and viscosity of lubricant used.

The focus of the present work is to study the performance of conical hydrodynamic journal bearing for various semi-cone angles and bridge the gap in the available open literature. In the present research work, finite element method is used to solve Reynolds equation and to compute the performance of conical hydrodynamic journal bearing for a wide range of radial load ($\bar{W}_r = 0.1 - 0.9$). The numerically simulated results have been presented for four conical hydrodynamic journal bearings having different semi-cone angles (γ = 5°, 10°, 20°, 30°) in terms of static and dynamic performance characteristics such as load-carrying capability, fluid film thickness, stiffness coefficients, damping coefficients and threshold speed of journal bearing. Based on this parametric study, hydrodynamic conical journal bearing is suggested as an option to replace the two separate journal bearings, i.e., cylindrical and thrust in applications, where radial and constant axial loads act on rotating shaft.

2 Analysis

Conical hydrodynamic journal bearing is analyzed using modified Reynolds equation in steady-state equilibrium condition for rotation of journal in the clearance space of bearing. Schematic view of a bearing supported by fluid film in clearance space is shown in Fig. 1. Bearing model is developed and expressed in spherical coordinate system. Time-dependent equation governing the fluid flow in the clearance space of conical hydrodynamic journal bearing is as follows:

$$\frac{1}{r}\frac{\partial}{\partial r}\left(\frac{r}{12\mu}h^3\frac{\partial p}{\partial r}\right)+\frac{1}{\sin^2\gamma}\frac{\partial}{\partial\phi}\left(\frac{h^3}{12\mu}\frac{1}{r^2}\frac{\partial p}{\partial\phi}\right)=\frac{\omega}{2}\frac{\partial h}{\partial\phi}+\frac{\partial h}{\partial t} \tag{1}$$

where r, γ, ω, μ, p and h represent the journal radius, semi-cone angle, journal rotational speed, viscosity of lubricating fluid, fluid pressure and fluid film thickness, respectively.

Equation (1) is expressed in non-dimensionalized form as follows (Sharma et al. 2011a, b):

$$\frac{\partial}{\partial\beta}\left((\sin^2\gamma)\beta\frac{\bar{h}^3}{12\bar{\mu}}\frac{\partial\bar{p}}{\partial\beta}\right)+\frac{\partial}{\partial\alpha}\left(\frac{1}{\beta}\frac{\bar{h}^3}{12\bar{\mu}}\frac{\partial\bar{p}}{\partial\alpha}\right)=\frac{\Omega}{2}\frac{\partial\bar{h}}{\partial\alpha}+\frac{\partial\bar{h}}{\partial\bar{t}} \tag{2}$$

where the following non-dimensional parameters are:

$$\beta=r\sin\gamma/R_J;\quad \bar{p}=p/p_s;\quad \bar{h}=h/c_r;\quad \bar{t}=t/\mu R_j^2/c_r^2p_s;$$
$$\Omega=\omega\left(\mu R_j^2/c_r^2p_s\right);$$

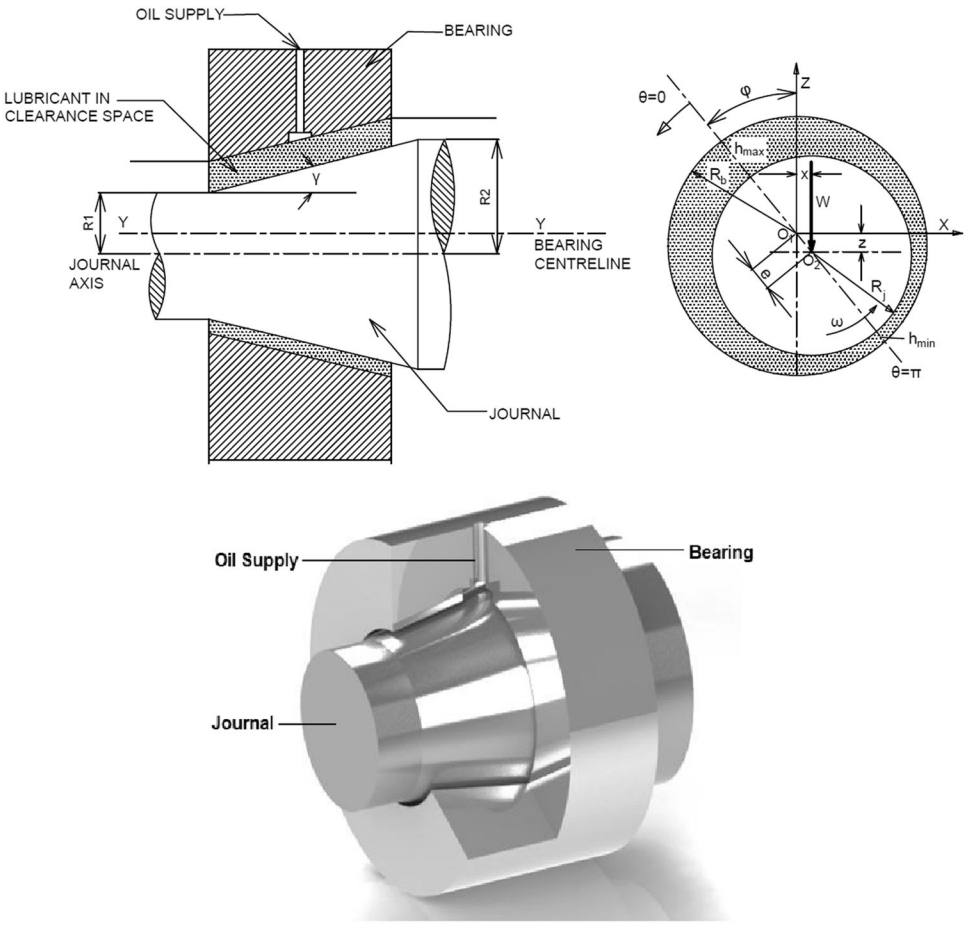

Fig. 1 Conical hydrodynamic journal bearing configuration in equilibrium position

c_r radial clearance; $\alpha = \phi$, circumferential coordinate (angle in radians); β axial coordinate of cone; $\bar{p}$ dimensionless pressure.

Flow field between the bearing and journal clearance space is discretized by using 60 nodes and 48 isoparametric elements in the present analysis and is shown in Fig. 2. In computational domain, each element is represented by the corresponding corner node number and the element is

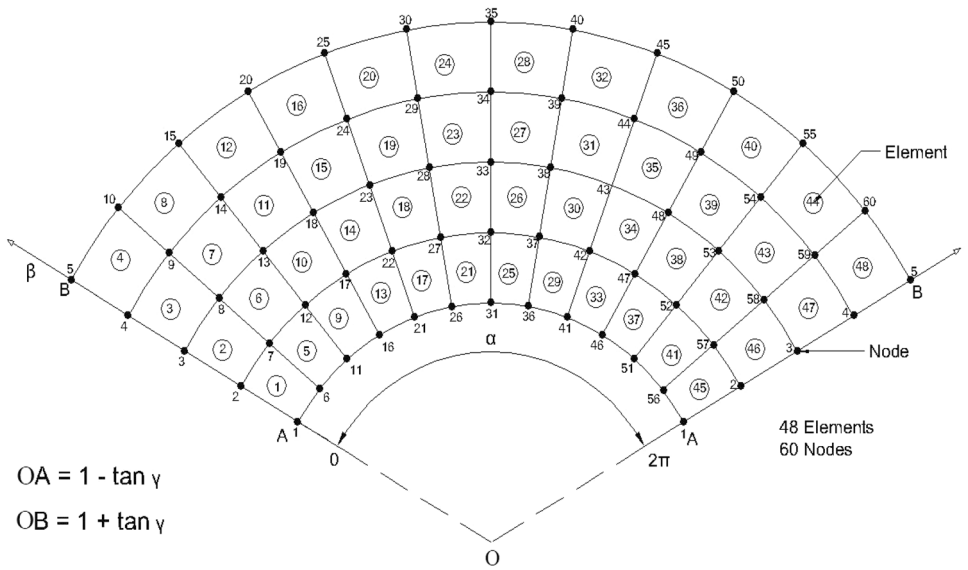

Fig. 2 FEA model of development surface of conical journal bearing

identified by the number at the center of the element. In finite element formulation, for simplicity and feasibility of the solution, this model is preferred and results are found to be converging with this model (Sharma et al. 2011a, b; Khakse et al. 2016).

Following Lagrangian interpolation function used for pressure calculation at nodal points by incorporating the boundary conditions:

$$\bar{p} = \sum_{j=1}^{4} N_j \bar{p}_j \tag{3a}$$

where N_j is the shape function for linearly interpolated isoparametric element.

Shape function N_j is expressed in terms of local coordinates (ξ, η) as follows:

$$\begin{aligned} N_1 &= \frac{1}{4}(1-\xi)(1-\eta) \\ N_2 &= \frac{1}{4}(1+\xi)(1-\eta) \\ N_3 &= \frac{1}{4}(1+\xi)(1+\eta) \\ N_4 &= \frac{1}{4}(1-\xi)(1+\eta) \end{aligned} \tag{3b}$$

$$\bar{p}^e = \left[N_1, N_2, N_3, N_4\right] \begin{Bmatrix} \bar{p}_1 \\ \bar{p}_2 \\ \bar{p}_3 \\ \bar{p}_4 \end{Bmatrix} \tag{3c}$$

Using the value of $\bar{p}$ in Eq. (2), and Galerkin's technique to minimize the residue by orthogonality condition along with interpolation function, then the typical element equation in matrix form is as follows:

$$[\bar{F}]^e\{\bar{P}\}^e = [\bar{Q}]^e + \Omega\{\bar{R}_{\mathrm{H}}\}^e + \dot{\bar{x}}_j\{\bar{R}_{x_j}\}^e + \dot{\bar{z}}_j\{\bar{R}_{z_j}\}^e \tag{4}$$

The resulting equation for all the elements are obtained and assembled in global matrix form, which can be expressed as follows:

$$[\bar{F}]\{\bar{P}\} = [\bar{Q}] + \Omega\{\bar{R}_{\mathrm{H}}\} + \dot{\bar{x}}_j\{\bar{R}_{x_j}\} + \dot{\bar{z}}_j\{\bar{R}_{z_j}\} \tag{5}$$

where $[\bar{F}]$ assembled fluidity matrix, $\{\bar{P}\}$ nodal pressure vector, $[\bar{Q}]$ nodal flow vector, $\{\bar{R}_{\mathrm{H}}\}$ column vectors due to hydrodynamic terms, $\{\bar{R}_{x_j}\}, \{\bar{R}_{z_j}\}$ global right-hand side vectors due to journal center linear velocities.

The total pressure at a node point (for jth node) in the lubricant flow field is given by the expression:

$$\bar{P}_j = \bar{P}_j\left(\bar{X}_j, \bar{Z}_j, \dot{\bar{X}}_j, \dot{\bar{Z}}_j\right) \tag{6}$$

where pressure is the function of journal steady-state position $(\bar{X}_J, \bar{Z}_J)$ and velocity condition $\left(\dot{\bar{X}}_J, \dot{\bar{Z}}_J\right)$. If initial steady-state position with zero initial velocity $(\dot{\bar{X}}_J = 0 = \dot{\bar{Z}}_J)$ is assumed, then initial flow field condition is as follows:

$$\bar{P}_j = \bar{P}_j(\bar{X}_J, \bar{Z}_J) = \bar{P}_o \tag{7}$$

where $\bar{P}_o$ steady-state nodal pressure

After modifications for necessary boundary conditions, Eq. (5) is solved for nodal pressure using linearized perturbation method applied to Reynolds equation.

2.1 Fluid Film Thickness

The fluid film thickness ($\bar{h}$) between clearance space of journal and bearing is expressed in a non-dimensional form (Sharma et al. 2011a, b) in the expression as shown in Eq. (8).

$$\bar{h} = \left(1 - \bar{X}_j \cos\alpha - \bar{Z}_j \sin\alpha\right)\cos\gamma \tag{8}$$

Assumptions made in this equation are: rigid bearing and journal surfaces, uniform axial and azimuthal clearance and journal is alignment in bearing configuration.

2.2 Boundary Conditions

In fluid film bearing, fluid film thickness (h) is very small as compared to the bearing length (L) and mean radius of journal (R_j), i.e., (h/L); (h/R_j)$\ll$1; hence, a negligible effect of film curvature on performance of bearing has been reported. The boundary conditions used for the analysis of lubricant flow field are described as follows by Luis (2010).

1. The pressure is periodic in the circumferential direction

$$\bar{p}(\alpha, \beta, t) = \bar{p}(\alpha + 2\pi, \beta, t) \tag{9a}$$

2. The pressure equals the atmospheric pressure on the bearing sides/edges

$$\bar{p}(\alpha, \beta = +1, t) = \bar{p}(\alpha, \beta = -1, t) = 1 \tag{9b}$$

3. Reynolds boundary conditions are employed for solution and assumed that pressure and pressure derivative are equal to zero at the outlet condition ($\alpha = \theta_2$).

$$\bar{p})_{\alpha=0} = 0; \quad \bar{p})_{\alpha=\theta_2} = 0; \quad \frac{\partial\bar{p}}{\partial\alpha})_{\alpha=\theta_2} = 0 \tag{9c}$$

$$\bar{p} \geq \bar{p}_{\mathrm{cav}}; \quad \text{in } 0 \leq \alpha \leq 2\pi; \quad \beta = -1 \leq z \leq \beta = +1 \tag{9d}$$

2.3 Load-Carrying Capacity

Figure 3 shows the external load impressed on the journal of a hydrodynamic conical journal bearing. The resultant components of load in axial and radial directions ($\bar{F}_a$, $\bar{F}_r$) are expressed in Eqs. (10a) and (10b) (Rajput and Sharma 2013).

$$\bar{F}_r = \bar{F}\cos\gamma = -\int_{-\lambda}^{\lambda}\int_{0}^{2\pi} \bar{p}\cos\gamma \; d\alpha d\beta \tag{10a}$$

$$\bar{F}_a = \bar{F}\sin\gamma = -\int_{-\lambda}^{\lambda}\int_{0}^{2\pi} \bar{p}\sin\gamma \; d\alpha d\beta \tag{10b}$$

In Eqs. (10c) and (10d), the resultant radial load ($\bar{F}_r$) acts on journal center at an angle θ as shown in Fig. 3, and it is further resolved into X and Z directions ($\bar{F}_x$ and $\bar{F}_z$) as follows:

$$\bar{F}_x = \bar{F}_r\cos\theta = -\int_{-\lambda}^{\lambda}\int_{0}^{2\pi} \bar{p}\cos\theta\cos\gamma \; d\alpha d\beta \tag{10c}$$

$$\bar{F}_z = \bar{F}_r\sin\theta = -\int_{-\lambda}^{\lambda}\int_{0}^{2\pi} \bar{p}\sin\theta\cos\gamma \; d\alpha d\beta \tag{10d}$$

2.4 Fluid Film Dynamic Coefficients

The fluid film stiffness coefficients ($\bar{S}_{ij}$) and damping coefficients ($\bar{C}_{ij}$) have been evaluated as a function of the relative displacements and velocities of the journal center with respect to bearing center, respectively. Fluid film reaction components on the journal are calculated by integration of the pressure field acting on the journal surface. The small magnitude of journal displacement ($\Delta\bar{X}_J, \Delta\bar{Z}_J$) about the journal position and fluid film replaced by dynamic coefficients of bearing is shown in Fig. 4.

The fluid film stiffness and damping coefficients ($\bar{S}_{ij}$, $\bar{C}_{ij}$) are defined as the negative rate of change in fluid film reaction with respect to film thickness and are expressed in Eqs. (11) and (12), respectively (Sharma et al. 2011b), which are functions of the journal center displacements and velocities in X and Z directions.

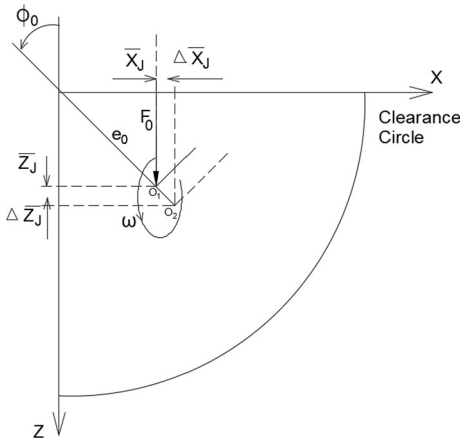

Fig. 4 The equilibrium locus of journal center of a fluid film hydrodynamic journal bearing

$$\bar{S}_{ij} = -\frac{\partial\bar{F}_i}{\partial\bar{q}_j} \tag{11}$$

$$\bar{C}_{ij} = -\frac{\partial\bar{F}_i}{\partial\dot{\bar{q}}_j} \tag{12}$$

where 'i' represents the direction of force or moment and $\bar{q}_j$ represents the direction of journal center displacement as ($\bar{q}_j = \bar{X}_j, \bar{Z}_j$). $\dot{\bar{q}}_j$ represents the velocity component of journal center ($\dot{\bar{q}}_j = \dot{\bar{X}}_j, \dot{\bar{Z}}_j$).

2.5 Stability Parameters of a Linearized System

The stability parameters such as threshold speed ($\bar{\omega}_{th}$) of journal bearing are obtained using the Routh's stability criteria. The threshold speed is obtained by using the relation as follows (Sharma and Rajput 2012):

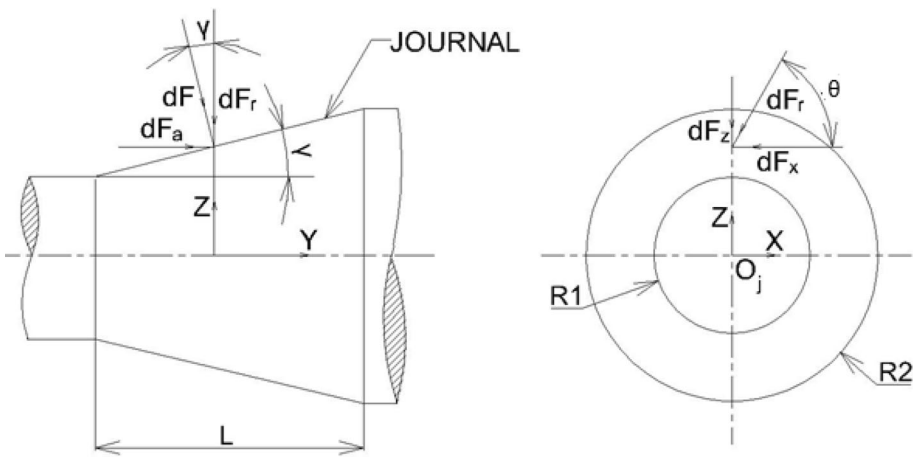

Fig. 3 Load-carrying capacity distribution of a conical journal bearing

$$\bar{\omega}_{\text{th}} = \left[\bar{M}_{\text{c}}/\bar{F}_0\right]^{1/2} \tag{13}$$

where $\bar{F}_0$ is resultant fluid film force $\left(\frac{\partial \bar{h}}{\partial \bar{t}} = 0\right)$.

A journal bearing is asymptotically stable when the operating speed of the journal is less than the threshold speed, i.e., when $(\Omega < \bar{\omega}_{\text{th}})$.

3 Solution Procedure

Finite element method is used to solve Reynolds equation governing the flow of lubricant in the clearance space of a conical journal and bearing. The solution of Eq. (5) has been obtained with steady-state conditions for journal center coordinates using the bearing geometric and operating parameters (Sharma et al. 2011a; Sharma and Rajput 2012) as shown in Table 1.

In the present study of conical hydrodynamic journal bearing, results are computed by the iterative procedure as follows (Sharma et al. 2011b):

- Computation of maximum pressure by solving Reynolds equation for lubricant flow
- Examination of journal center equilibrium position
- Computation of static and dynamic performance characteristics.

The increment in journal center coordinates is used to calculate the nodal values of fluid film thickness, and thereafter, the fluidity matrices are generated for each element. The system equation for specified boundary conditions is directly solved for the nodal pressure using the Gaussian elimination technique. The computation of nodal pressure requires system fluidity matrix with the continuity of flow between journal and bearing. The solution of system equation to establish the equilibrium journal center position has been obtained for *i*th journal center position using the following equations:

$$\begin{aligned} \bar{F}_x &= 0 \\ \bar{F}_z &= \bar{W}_{\text{r}} \end{aligned} \tag{14}$$

The new coordinates for journal center $\left(\bar{X}_J^{i+1}, \bar{Z}_J^{i+1}\right)$ are represented as:

$$\begin{aligned} \bar{X}_J^{i+1} &= \bar{X}_J^i + \Delta\bar{X}_J^i \\ \bar{Z}_J^{i+1} &= \bar{Z}_J^i + \Delta\bar{Z}_J^i \end{aligned} \tag{15}$$

where $\bar{X}_J^i$, $\bar{Z}_J^i$ are the coordinates of the journal center position as shown in Fig. 4. The iterative solutions were continued until the following convergence criterion was satisfied:

$$\left[\frac{\left(\left(\Delta\bar{X}_J^i\right)^2 + \left(\Delta\bar{Z}_J^i\right)^2\right)^{1/2}}{\left(\left(\bar{X}_J^i\right)^2 + \left(\bar{Z}_J^i\right)^2\right)^{1/2}}\right] 100 < 0.001 \tag{16}$$

Fluid film thickness $(\bar{h})$ at all node points is computed assuming the bearing as a rigid body, and the results for this are used as input parameters for computing nodal pressure. The iterative solution procedure shown in Fig. 5 is used for the computation of static and dynamic performance characteristics.

Table 1 Operating and geometric parameters for conical hydrodynamic journal bearing

Bearing parameters	Value
Aspect ratio ($\lambda = L/D$)	1.0
Mean journal radius (R_j) (mm)	50
Bearing length (L) (mm)	100
Clearance ratio (c_r/R_j)	0.001
Bearing profile—conical (γ) (semi-cone angle)	5°, 10°, 20°, 30°
Radial load ($\bar{W}_{\text{r}}$)	0.1–0.9
Supply pressure (p_{s}) (MPa)	0.5
Relative velocity/speed (v) (m/s)	2.6
Lubricant viscosity (μ) (Pa s)	0.0277
Lubricant density (ρ) (kg/m^3)	860

4 Results and Discussion

In the present work, the performance of the conical hydrodynamic journal bearings with semi-cone angles (γ = 5°, 10°, 20°, 30°) has been investigated for a range of radial load ($\bar{W}_{\text{r}} = 0.1 - 0.9$). Presented results have been discussed in terms of maximum fluid film pressure, radial and axial load-carrying capacity, minimum fluid film thickness, stiffness coefficients, damping coefficients and threshold speed of conical journal bearing. The influence of various operating and geometric parameters on bearing has been numerically simulated using the analytical model and code developed in Fortran-77.

The numerically computed results in the present study have been compared in two stages. In the first stage, numerical simulated results were compared with results obtained by using the ANSYS Fluent software in CFD analysis, and in the second stage numerical simulated results were compared with experimental results. A comparison of non-dimensional maximum pressure for conical hydrodynamic journal bearing (γ = 10°) and aspect ratio (λ =1) for the CFD model as shown in Fig. 6a indicates a good agreement between the numerically calculated FEA results at a journal speed of 2000 rpm as shown in Fig. 6b.

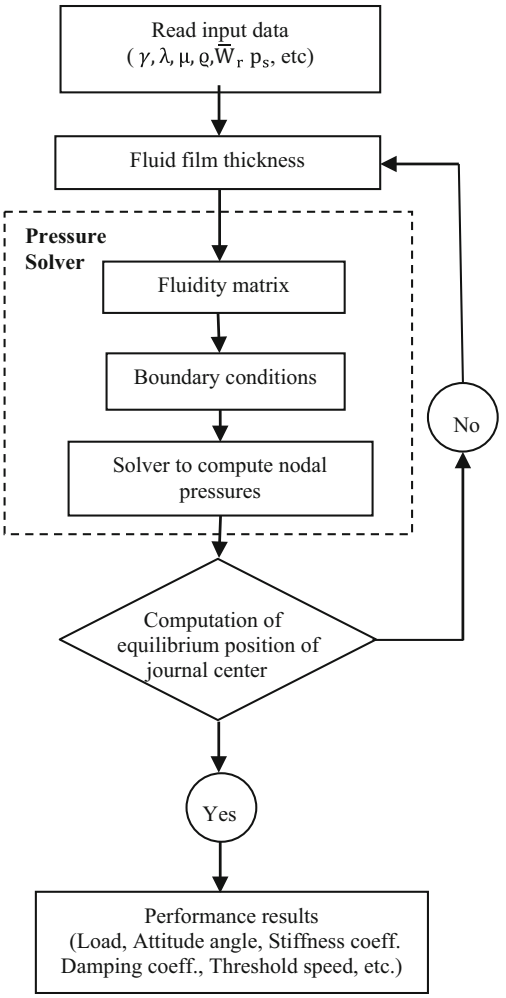

Fig. 5 Flowchart for computation of performance of static and dynamic characteristics

In the second stage of validation, the numerically stimulated results have been validated on customized manufactured conical hydrodynamic journal bearing test rig (CHJB-test-rig) for a semi-cone angle 10° and aspect ratio (λ =1) at the Machine Dynamics and Vibration Laboratory, VJTI, Mumbai, India. The CHJB-test-rig devised for this purpose is capable of measuring the pressure distribution at selected points in conical journal bearing, as shown in Fig. 7. In CHJB-test-rig, all physically relevant parameters have been taken into account the FEA simulation model of conical journal bearing for semi-cone angle 10°. On the circumference of conical bearing, at the mid-plane eight predefined positions are used for instrumentations as shown in Fig. 7b. In this study, five ports (Nos. P_1, P_2, P_3, P_4 and P_5) are used for measuring the pressure, two ports (Nos. T_1 and T_2) are used for temperature measurement and one port (IP_1) is utilized for oil supply to the bearing. The experimental results for pressure at these positions have been compared with the FEA results. Figure 8 shows a good agreement between numerical and experimental results.

4.1 Variation of Maximum Pressure ($\bar{P}_{max}$) with Radial Load ($\bar{W}_r$)

Maximum pressure ($\bar{P}_{max}$) developed in fluid film conical hydrodynamic journal bearing for various semi-cone angles (γ =5°, 10°, 20°, 30°) with variation in radial load condition is as shown in Fig. 9. Conical hydrodynamic journal bearing with semi-cone angle 5° has higher specific load (W/L^*D) as compared to bearing of semi-cone angle 30° for the same mean diameter and bearing axial length. Thus,

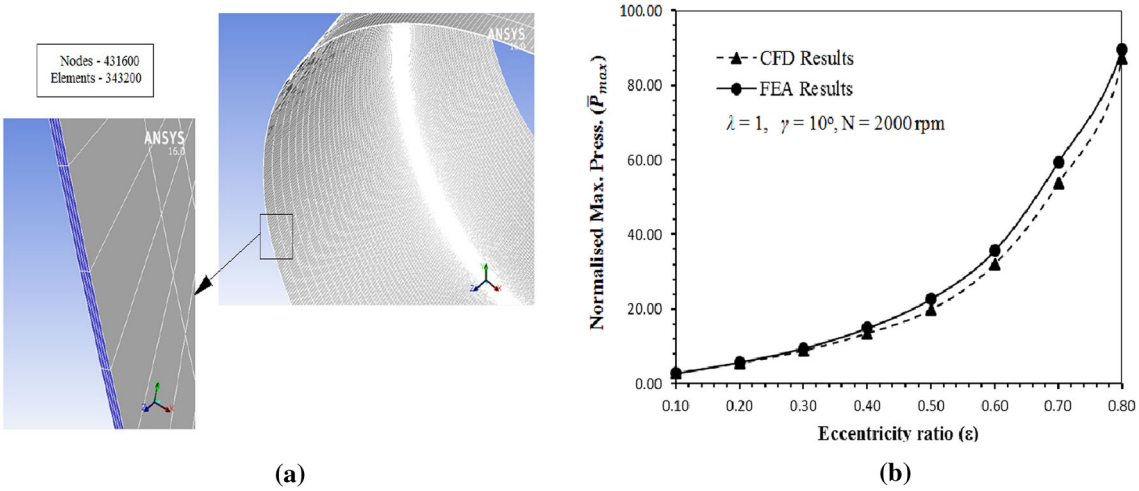

(a) **(b)**

Fig. 6 Validation of proposed analytical model with CFD results. **a** CFD model of conical hydrodynamic journal bearing (semi-cone angle = 10°). **b** Normalized Max. Press. ($\bar{P}_{max}$) versus eccentricity ratio (ε) at the mid-plane of conical hydrodynamic journal bearing

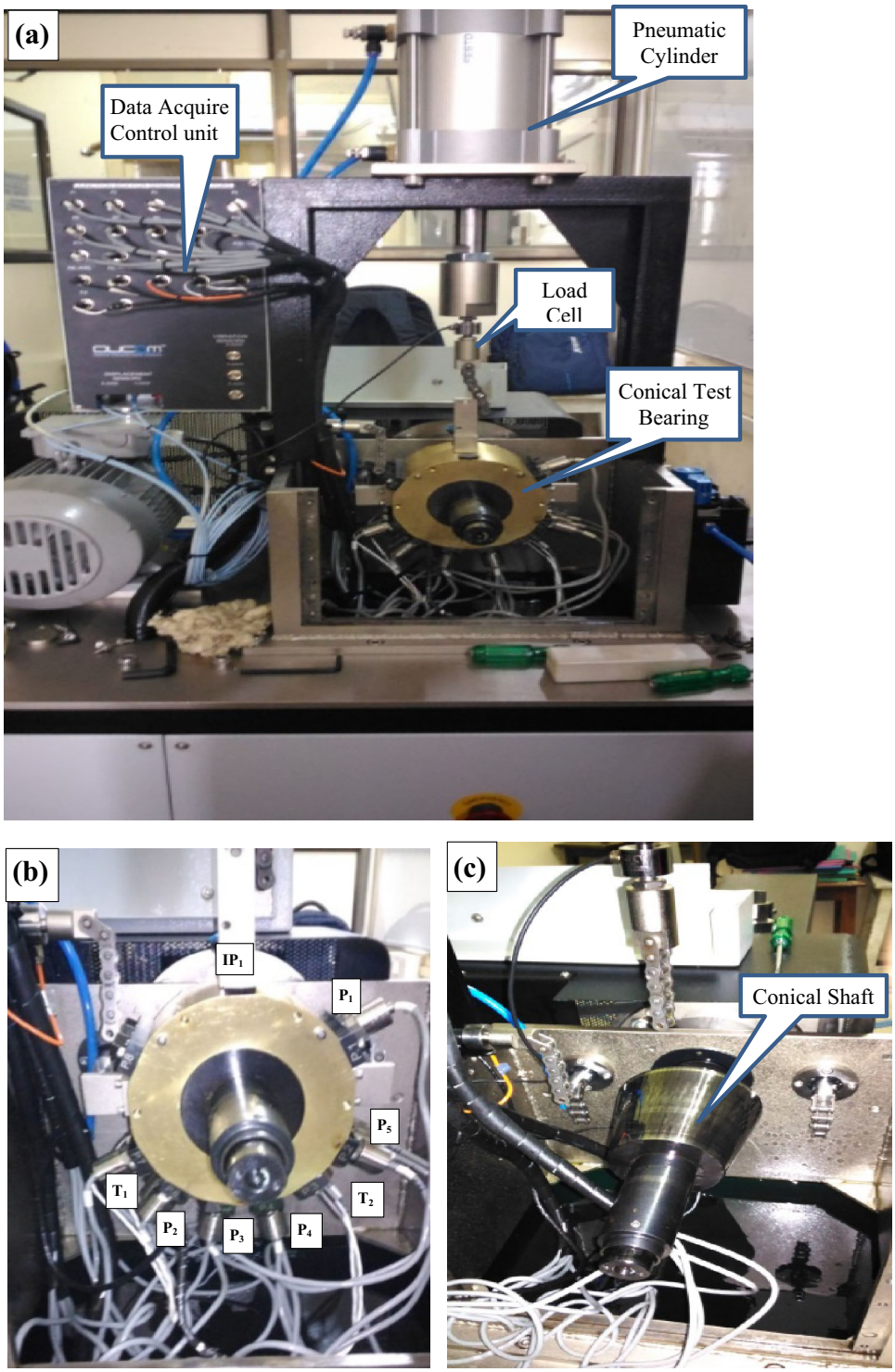

Fig. 7 **a** Conical hydrodynamic journal bearing (CHJB)-test-rig, at VJTI, Mumbai. **b** Conical test bearing with eight ports for mounting the pressure and temperature sensors. **c** Conical shaft of semi-cone angle ($\gamma = 10°$)

in order to support the same value of the radial load ($\bar{W}_r$), the required fluid film pressure is reduced with the increase in the semi-cone angle from 5° to 30° for bearing of aspect ratio ($\lambda = 1$). Therefore, from this viewpoint conical hydrodynamic journal bearing of semi-cone angle 30° is most suitable for variation in radial load application as compared to the other configurations of conical bearings studied. It is depicted from Fig. 9 that $\bar{P}_{max}$ is reduced in the order of 29.13, 18.88 and 6.93%, for conical bearing of semi-cone angles 30°, 20° and 10° as compared to base bearing of semi-cone angle 5°, respectively, when bearing is operating at radial load ($\bar{W}_r$) equal to 0.9. However, it was also observed that the value of maximum pressure ($\bar{P}_{max}$) increases linearly with the increase in radial load

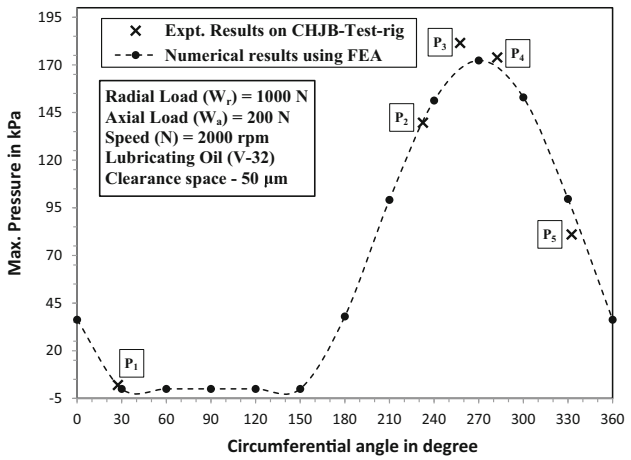

Fig. 8 Validation of FEA model/algorithm results with experimental results on customized CHJB-test-rig of semi-cone angle (γ = 10°) and aspect ratio (λ =1)

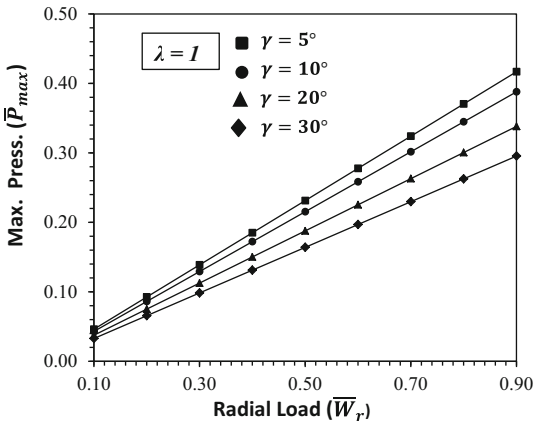

Fig. 9 Variation of maximum pressure ($\bar{P}_{max}$) w.r.t. radial load ($\bar{W}_r$); speed (v = 2.6 m/s)

($\bar{W}_r$) from 0.1 to 0.9 for all four configurations of conical journal bearings. Further, generally, when the bearing operates under higher load condition ($\bar{W}_r = 0.9$), the pressure developed in bearing of semi-cone angle 30° is significant as compared to bearing operating in low load condition ($\bar{W}_r \leq 0.3$), with respect to base bearing of semi-cone angle 5°.

4.2 Variation of Axial Load ($\bar{W}_a$) with Radial Load ($\bar{W}_r$)

When a radial load is applied to a conical fluid film journal bearing, the load is transmitted from the bearing to conical journal through the fluid film and the reaction from the fluid film is developed at normal to the conical surface. This reactive force induces a component in axial direction, which is influenced by the semi-cone angle of conical bearing. From the results, it is observed that for all four configurations of bearings, capability to resist the load in axial direction ($\bar{W}_a$) has increased with the increase in semi-cone angle. It is observed in Fig. 10 that for a conical bearing of semi-cone angles (10°, 20° and 30°), there is increase in the value of $\bar{W}_a$ in order of 2.01, 4.16 and 6.6 times, respectively, with respect to base bearing of semi-cone angle of 5° for aspect ratio (λ =1) and bearing operating at radial load ($\bar{W}_r$) equal to 0.9.

4.3 Variation of Fluid Film Thickness ($\bar{h}_{min}$) with Radial Load ($\bar{W}_r$)

In order to support the same value of external vertical load in conical hydrodynamic journal bearing, the fluid film thickness decreases with the increase in semi-cone angles. This is also confirmed by the fact that for a conical journal bearing, fluid film thickness is a function of the cosine of semi-cone angle. Therefore, the fluid film thickness reduces with the increase in semi-cone angles, and Fig. 11 depicts that the bearing of semi-cone angle 30° provides less value of $\bar{h}_{min}$ as compared to base bearing of semi-cone angle 5°. In specific applications, where bearings are placed inside the machine and replacement is not easy, there is a need to ensure minimum film thickness to avoid initiation of wear and metal-to-metal contact at contact surfaces. It has been also observed from Fig. 11 that the influence of semi-cone angle 30° on the value of $\bar{h}_{min}$ is significantly higher as compared to bearing having the semi-cone angles 5°, 10° and 20°. It is seen from results that for semi-cone angles 10°, 20° and 30°, the value of $\bar{h}_{min}$ decreases in the order of 0.5, 3.57 and 9.84% with respect to base bearing, respectively, when bearing is operating at a radial load ($\bar{W}_r$) of 0.9 and aspect ratio (λ =1). Further, the percentage decrease in the value of the minimum fluid film thickness ($\bar{h}_{min}$) for radial load ($\bar{W}_r$) from 0.1 to 0.9 in case of conical journal bearing of semi-

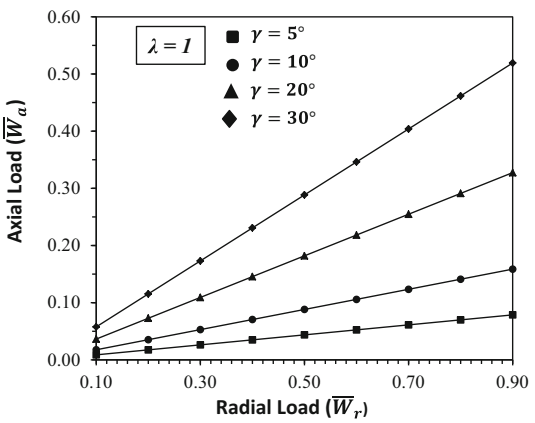

Fig. 10 Variation of axial load ($\bar{W}_a$) w.r.t. radial load ($\bar{W}_r$); speed (v = 2.6 m/s)

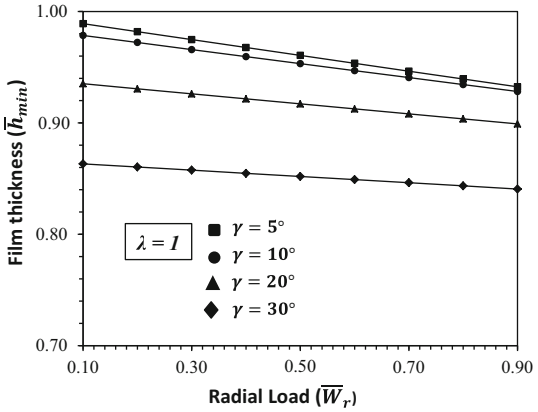

Fig. 11 Variation of film thickness ($\bar{h}_{\min}$) w.r.t. radial load ($\bar{W}_r$); speed (v = 2.6 m/s)

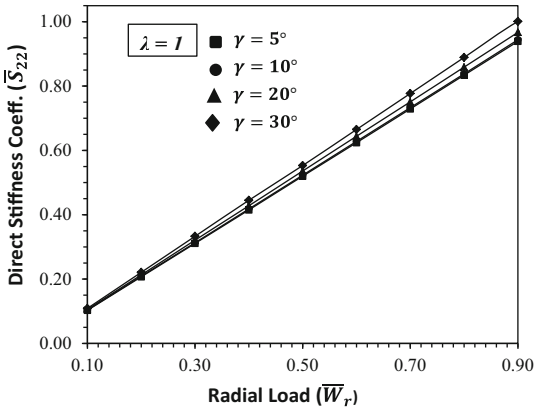

Fig. 13 Variation of direct stiffness coefficient ($\bar{S}_{22}$) versus radial load ($\bar{W}_r$); speed (v = 2.6 m/s)

cone angle 30° is found to be less than 50% with respect to base bearing of semi-cone angle 5° which appears to be quite significant. Therefore, conical journal bearing of semi-cone angle of 30° has been found more consistent for the various load conditions as compared to other configurations of conical bearing studied.

4.4 Variation of Direct Stiffness Coefficient ($\bar{S}_{11}$, $\bar{S}_{22}$) with Radial Load ($\bar{W}_r$)

The influence of radial load on direct stiffness coefficient in X direction ($\bar{S}_{11}$) and in Z direction ($\bar{S}_{22}$) for various configurations of conical journal bearing (γ =5°, 10°, 20°, 30°) is shown in Figs. 12 and 13, respectively. The value of fluid film reaction components in radial and axial directions changes with the increase in the value of semi-cone angle (γ), and accordingly, the values of fluid film stiffness coefficients are anticipated to change. Figure 12 depicts that for hydrodynamic conical journal bearing of aspect ratio (λ =1) and for radial load condition ($\bar{W}_r = 0.9$), the value of $\bar{S}_{11}$ increases in the order of 0.9, 4.38 and 10.51% for the bearing of semi-cone angles 10°, 20° and 30° with respect to the base bearing of semi-cone angle 5°, respectively. Further, Fig. 13 indicates that for the same operating conditions, the value of $\bar{S}_{22}$ increases in the order of 0.5, 2.98 and 6.6% for conical bearing of semi-cone angles 10°, 20° and 30° with respect to base bearing of semi-cone angle 5°, respectively, as shown in Fig. 13. For all the configurations used for study of conical journal bearing, the value of direct fluid film stiffness coefficients ($\bar{S}_{11}$, $\bar{S}_{22}$) is observed to be largest for the semi-cone angle 30° as compared to base bearing of semi-cone angle 5° for all the operating load conditions under study. The increase in the value of direct fluid film stiffness coefficient indicates better dynamic stability of conical hydrodynamic journal bearing for varying radial load conditions.

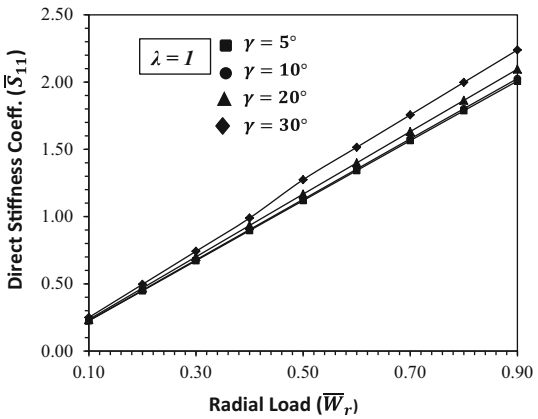

Fig. 12 Variation of direct stiffness coefficient ($\bar{S}_{11}$) w.r.t. radial load ($\bar{W}_r$); speed (v = 2.6 m/s)

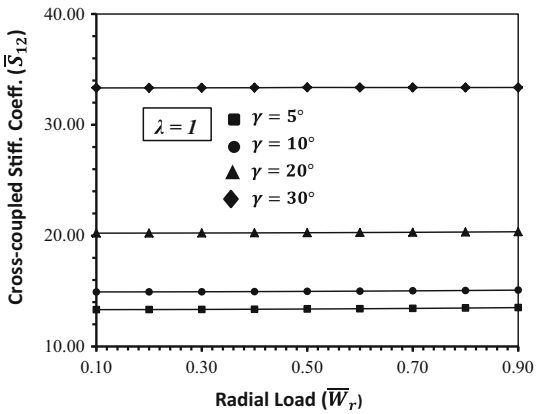

Fig. 14 Variation of cross-coupled stiff. coeff. ($\bar{S}_{12}$) w.r.t. radial load ($\bar{W}_r$); speed (v = 2.6 m/s)

4.5 Variation of Cross-Coupled Stiffness Coefficient ($\bar{S}_{12}$, $\bar{S}_{21}$) with Radial Load ($\bar{W}_r$)

Variation of cross-coupled stiffness coefficients ($\bar{S}_{12}$, $\bar{S}_{21}$) is shown in Figs. 14 and 15 for semi-cone angles (γ =5°, 10°, 20°, 30°). The value of $\bar{S}_{12}$ for a bearing with aspect ratio (λ =1) and semi-cone angles 10°, 20° and 30° increases in the order of 11.67, 50.66 and 147.04% with respect to base bearing of 5°, respectively, when bearing is operating at radial load ($\bar{W}_r = 0.9$) as shown in Fig. 14. While for the same operating conditions, the value of $\bar{S}_{21}$ is decreased in the order of 12.52, 56.56 and 149.92% for the bearing of semi-cone angles 10°, 20° and 30° with respect to base bearing, respectively. Results also show that cross-coupled stiffness coefficients significantly influenced the performance and stability of conical journal bearing at higher semi-cone angles. Further, it has been observed under steady state, at a constant journal speed of 2.6 m/s. Cross-coupled stiffness coefficients ($\bar{S}_{12}$, $\bar{S}_{21}$) are not influenced by change in radial load. It is also observed that stiffness coefficients increase with the increase in semi-cone angles and this is due to fact that the quantity of lubricant increases in clearance space with the increase in semi-cone angle.

4.6 Variation of Direct Damping Coefficients ($\bar{C}_{11}$, $\bar{C}_{22}$) with Radial Load ($\bar{W}_r$)

Direct damping coefficients ($\bar{C}_{11}$, $\bar{C}_{22}$) counterbalance the effect of cross-coupled stiffness coefficients and improve the performance of the bearing. The damping coefficients depend on the viscosity of the fluid film and equilibrium position of the journal. The variation of direct fluid film damping coefficients ($\bar{C}_{11}$, $\bar{C}_{22}$) is shown in Figs. 16 and 17, respectively. It is illustrated in Fig. 16 that bearing with semi-cone angle of 30° has higher effective damping as compared to base bearing of semi-cone angle 5° from the point of view of damping out the oscillations, as the bearing with semi-cone angle 30° provides the larger value of direct fluid film damping coefficients ($\bar{C}_{11}$, $\bar{C}_{22}$) among all the configuration of bearings studied. The value of $\bar{C}_{11}$ is increased in the order of 10.50, 43.55 and 118.52% for semi-cone angle of 10°, 20° and 30° with respect to base bearing, respectively, when bearing is operating at load condition ($\bar{W}_r = 0.9$) for conical hydrodynamic journal bearing of aspect ratio (λ =1), whereas for the same operating conditions the value of $\bar{C}_{22}$ is found to be increased in the order of 11.41, 48.98 and 122.84% for the bearing of semi-cone angles 10°, 20° and 30° with respect to base bearing of semi-cone angle 5°, respectively, as shown in Fig. 17. Further, it has been observed under steady state, at a constant journal speed of 2.6 m/s. The value of direct fluid film damping coefficients ($\bar{C}_{11}$, $\bar{C}_{22}$) is not influenced by change in radial load for all the configurations of bearings studied.

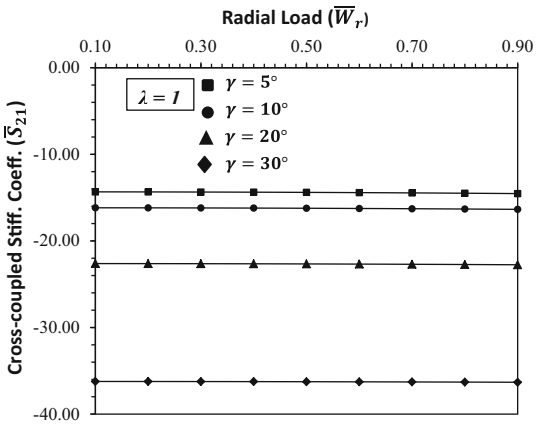

Fig. 15 Variation of cross-coupled stiff. coeff. ($\bar{S}_{21}$) w.r.t. radial load ($\bar{W}_r$); speed (v = 2.6 m/s)

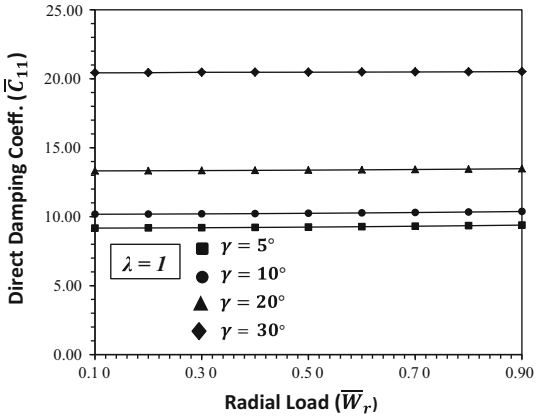

Fig. 16 Variation of direct damping coefficient ($\bar{C}_{11}$) w.r.t. radial load ($\bar{W}_r$); speed (v = 2.6 m/s)

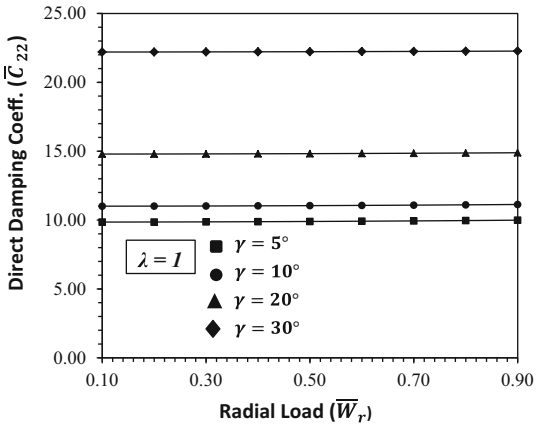

Fig. 17 Variation of direct damping coefficient ($\bar{C}_{22}$) w.r.t. radial load ($\bar{W}_r$); speed (v = 2.6 m/s)

4.7 Variation of Cross-Coupled Damping Coefficient ($\bar{C}_{12}$, $\bar{C}_{21}$) with Radial Load ($\bar{W}_r$)

The effect of variation in radial load on cross-coupled damping coefficients ($\bar{C}_{12}$, $\bar{C}_{21}$) is shown for semi-cone angles (γ =5°, 10°, 20°, 30°) in Figs. 18 and 19. In most of the analysis, for fluid film bearings cross-coupled fluid film damping coefficients have been computed, but for the sake of brevity, the performance characteristics have not been presented. However, these coefficients influenced the dynamic response of hydrodynamic conical journal bearing and are reported herewith. The value of $\bar{C}_{12}$ is found to decrease in the order of 1.4, 6.55 and 9.02% for semi-cone angle of 10°, 20° and 30° with respect to the base bearing, respectively, for aspect ratio (λ =1) and load condition ($\bar{W}_r = 0.9$) as exhibited in Fig. 17. While for the same operating conditions, $\bar{C}_{21}$ decreases in the order of 1.4, 6.67 and 21.14% for semi-cone angle of 10°, 20° and 30° with respect to base bearing, respectively, as presented in Fig. 18. Further, it has been observed that the value of cross-coupled damping coefficients ($\bar{C}_{12}$, $\bar{C}_{21}$) is decreased with the increase in radial load for all four configurations of conical journal bearing.

4.8 Variation of Threshold Speed Margin ($\bar{\omega}_{th}$) with Radial Load ($\bar{W}_r$)

The variations of threshold speed margin ($\bar{\omega}_{th}$) with variation in radial load for various semi-cone angles (γ =5°, 10°, 20°, 30°) are shown in Fig. 20. It has been observed that for a bearing of aspect ratio (λ =1) and semi-cone angle of 10°, 20° and 30°, the value of $\bar{\omega}_{th}$ decreases in the order of 0.7, 3.32 and 5.15%, respectively, with respect to base bearing when bearing is operating at load condition ($\bar{W}_r$) of 0.9. Conical bearing of semi-cone angle 30° has

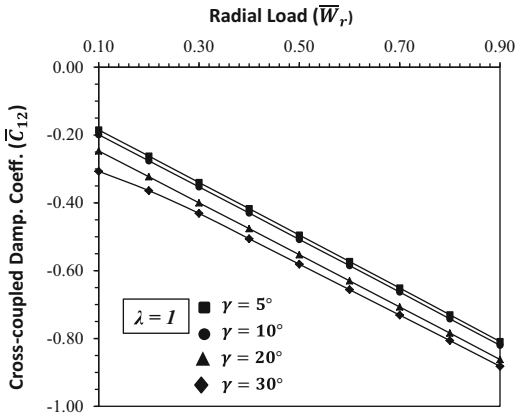

Fig. 18 Variation of cross-coupled damp. coeff. ($\bar{C}_{12}$) w.r.t. radial load ($\bar{W}_r$); speed (v = 2.6 m/s)

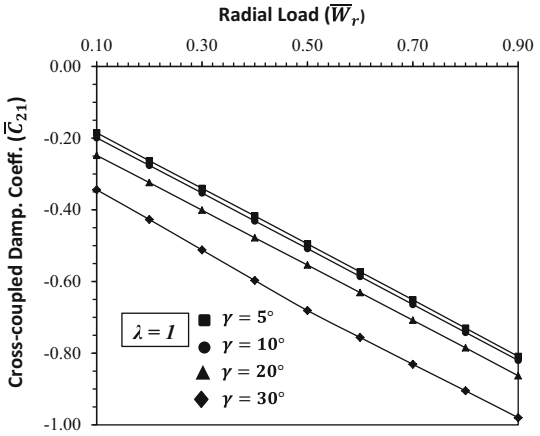

Fig. 19 Variation of cross-coupled damp. coeff. ($\bar{C}_{21}$) w.r.t. radial load ($\bar{W}_r$); speed (v = 2.6 m/s)

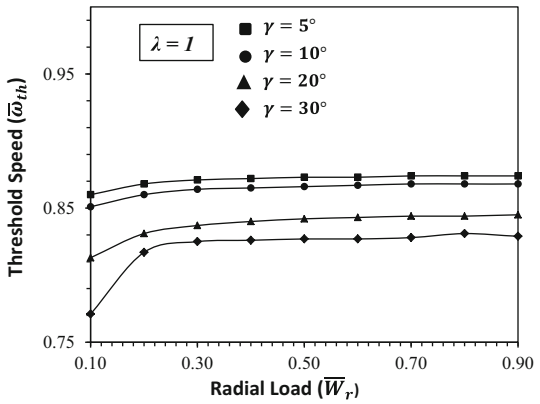

Fig. 20 Variation of threshold speed ($\bar{\omega}_{th}$) w.r.t. radial load ($\bar{W}_r$); speed (v = 2.6 m/s)

slightly longer bearing length as compared to base bearing of semi-cone angle 5° and has higher effective damping; therefore, the threshold speed of semi-cone angle 30° is low at the start. It is depicted from the trends in Fig. 20 that threshold speed margin ($\bar{\omega}_{th}$) is influenced at the start of the radial load in conical journal bearing. Also, there are some problems associated with lightly loaded bearings. Hence, low trends for all the configurations of bearings continue till $\bar{W}_r$ = 0.3. Later, sufficient lubricant layers are developed in bearing to provide nearly constant threshold speed over $\bar{W}_r$ = 0.3 to 0.9.

5 Conclusion

Performance analysis of conical hydrodynamic journal bearing for four semi-cone angles (γ =5°, 10°, 20°, 30°) is performed by using finite element method for varying load conditions ($\bar{W}_r = 0.1 - 0.9$). The conclusions drawn on the basis of the presented study are as follows:

1. With the increase in semi-cone angle from 5° to 30°, the required pressure in clearance space of fluid film bearing is decreased significantly to balance the radial load ($\bar{W}_r$) on bearing. It is also observed that for conical bearings, capability to resist the load in axial direction ($\bar{W}_a$) has increased with the increase in semi-cone angle.
2. Minimum fluid film thickness of bearing decreases with the increase in semi-cone angle from 5° to 30°, and it is observed that change in minimum fluid film thickness ($\bar{h}_{min}$) is more significant with the increase in semi-cone angle of the bearing.
3. Direct fluid film stiffness coefficients ($\bar{S}_{11}$, $\bar{S}_{22}$) increase with the increase in semi-cone angle. It is also observed that cross-coupled stiffness coefficient $\bar{S}_{12}$ increases with the increase in semi-cone angle, while the $\bar{S}_{21}$ decreases with the increase in semi-cone angle.
4. The value of damping coefficients ($\bar{C}_{11}$, $\bar{C}_{22}$) increases with the increase in semi-cone angle, whereas cross-coupled damping coefficients ($\bar{C}_{12}$, $\bar{C}_{21}$) decrease with the increase in semi-cone angle. The conical journal bearing with a higher value of semi-cone angle is better for damping-out oscillations.
5. The stability behavior for conical hydrodynamic journal bearing in terms of threshold speed ($\bar{\omega}_{th}$) decreases with the increase in semi-cone angle from base bearing of semi-cone angle 5° to other bearings of semi-cone angles 10°, 20° and 30°. It is also observed that the threshold speed ($\bar{\omega}_{th}$) shows variations for initial radial load ($\bar{W}_r$) condition up to 0.3 and thereafter shows almost constant behavior with the increase in radial load ($\bar{W}_r$) up to 0.9 for bearing of aspect ratio ($\lambda = 1$). The value of $\bar{\omega}_{th}$ decreases in the order of 5.15% for conical journal bearings of semi-cone angle 30° with respect to base bearing of semi-cone angle 5°, when bearing is operating at load condition ($\bar{W}_r$) of 0.9.

The present parametric study of conical hydrodynamic journal bearing is useful at preliminary design stage to substitute assemblies of journal and thrust bearing when the axial force has a constant value.

Acknowledgements The financial support from the All India Council for Technical Education (AICTE), New Delhi, India, under Research Promotion Scheme (RPS) Ref. No. 8-221/RIFD/RPS/Policy-1/2014-15 is gratefully acknowledged. The author is grateful to the Director, Veermata Jijabai Technological Institute (V.J.T.I), Mumbai, and Principal, K. J. Somaiya College of Engineering (KJSCE), Mumbai, for all support provided for this study which is respectfully acknowledged.

References

Benasciutti D, Gallina M, Munteanu MG, Flumian F (2012) A numerical approach for static and dynamic analysis of deformable journal bearings. World Acad Sci Eng Technol 67:778–783

Bouyer J, Fillon M (2011) Experimental measurement of the friction torque on hydrodynamic plain journal bearings during start-up. Tribol Int 44:772–781

Chen WJ (2012) Rotordynamics and bearing design of turbochargers. Mech Syst Signal Process 29:77–89

Cong S, Khonsari MM (2013) Effect of dimple's internal structure on hydrodynamic lubrication. Tribol Lett 52(1):415–430

Ettles C, Svoboda O (1975) The application of double conical journal bearings in high speed centrifugal pumps—parts 1 and 2. Proc Inst Mech Eng 189(1):221–230

Ferron J, Frene J, Boncompain R (1983) A study of the thermohydrodynamic performance of a plain journal bearing comparison between theory and experiments. Trans ASME 105:422–428

Gamal MAR, Al-Hanaya AM (2014) MHD flow of a non-Newtonian power law through a conical bearing in a porous medium. J Mod Phys 5:61–67

Heshmat H, Hunsberger AZ, Jahanmir S, Walton JF (2006) Prediction of hydrodynamic bearing performance for cardiac assist devices. ASAIO J 52(2):51A

Hong G, Xinmin L, Shaoqi C (2009) Theoretical and experimental study on dynamic coefficients and stability for a hydrostatic/hydrodynamic conical bearing. ASME J Tribol 131(701):1–7

Jagadeesha KM, Nagaraju T, Sharma SC, Jain SC (2012) 3D surface roughness effects on transient non-Newtonian response of dynamically loaded journal bearings. Tribol Trans 55(1):32–42

Khakse PG, Phalle VM, Mantha SS (2016) Performance analysis of a nonrecessed hybrid conical journal bearing compensated with capillary restrictors. Trans ASME J Tribol 138:011703-1–011703-9

Kim H, Jang G, Ha H (2012) A generalized Reynolds equation and its perturbation equations for fluid dynamic bearings with curved surfaces. Tribol Int 50:6–15

Kim K, Lee M, Lee S, Jang G (2017) Optimal design and experimental verification of fluid dynamic bearings with high load capacity applied to an integrated motor propulsor in unmanned underwater vehicles. Tribol Int 114:221–233

Kirk RG, Gunter EJ (1976) Short bearing analysis applied to rotor dynamics journal of engineering for industry. Trans ASME 98:576–592

Korneev AY (2014) Rigid-rotor dynamics of conical hydrodynamic bearings. Russ Eng Res 34:131–135

Korneev AYu, Yaroslavtsev MM (2010) Dynamic characteristics of conical multiple pad hydrodynamic liquid friction bearings. Russ Eng Res 30(4):365–369

Korneev AYu, Savin LA, Yaroslavtsev MM (2010) Static characteristics of conical multiple wedge hydrodynamic liquid friction bearings. Russ Eng Res 30(3):219–223

Krzysztof W (2008) Enhancement of memory capacity in HDD micro-bearing with hyperbolic journals. J KONES Powertrain and Transp 15(3):555–560

Luis SA (2010) Hydrodynamic fluid film bearings and their effect on the stability of rotating machinery. Texas A&M University College Station, TX 77843-3123, RTO-EN-AVT-143, pp 10-1–10-36

Mehrjardi MZ, Rahmatabadi AD, Meybodi RR (2016) A study on the stability performance of noncircular lobed journal bearings with micropolar lubricant. Proc Inst Mech Eng Part J Eng Tribol 230(1):14–30

Murthy TSR (1981) Analysis of multi-scallop self-adjusting conical hydrodynamic bearings for high precision spindles. Tribol Int 301:147–150

Papadopoulos CA, Nikolakopoulos PG, Gounaris GD (2008) Identification of clearances and stability analysis for a rotor-journal bearing system. Mech Mach Theory 43:411–426

Rajput AK, Sharma SC (2013) Analysis of externally pressurized multirecess conical hybrid journal bearing system using micropolar lubricant. Proc Inst Mech Eng Part J Eng Tribol 227(9):943–961

Sharma SC, Rajput AK (2012) Influence of micropolar lubrication on the performance of 4-pocket capillary compensated conical hybrid journal bearing. Adv Tribol 2012:898252. https://doi.org/10.1155/2012/898252

Sharma SC, Phalle VM, Jain SC (2011a) Performance analysis of a multi-recess capillary compensated conical hydrostatic journal bearing system. Tribol Int 44:617–626

Sharma SC, Phalle VM, Jain SC (2011b) Influence of wear on the performance of a multirecess conical hybrid journal bearing compensated with orifice restrictor. Tribol Int 44:1754–1764

Sumikura H, Fukunaga K, Funakubo A, Fukui Y (2005) Development of an axial flow blood pump with hydrodynamic conical bearings. ASAIO J 51(2):34A

Sumikura H, Fukunaga K, Funakubo A, Fukui Y (2006) Improvement and evaluation of an enclosed-impeller type axial flow blood pump with hydrodynamic conical bearings. ASAIO J 52(2):32A